International Journal of Science and Research (IJSR)
ISSN: 2319-7064
SJIF (2019): 7.583

Controller Design for CubeSat Attitude Control with BLDCM and Raction Wheels

Kuei-Tsun Chen

11 F-1, No. 69, Longxing St., Banqiao Dist., New Taipei City, 220 Taiwan (R.O.C.)
kueitsunchen[at]gmail.com

Abstract: ***For all satellites, attitude, orientation and orbit-propagation are critical to mission success. The attitude control system (ACS) usually has different operation modes for various situations of the task; for example, detumbling, three-axis stabilization, pointing... etc. The purpose of this article is to establish a dynamic mathematical model for simulating a small satellite in Low-Earth Orbit (LEO), and to design relevant controllers to implement attitude-pointing. In particular, the CubeSat applies a permanent magnet brushless DC-motor (BLDCM) connected with a reaction-wheel as an actuator, which generates control torque imposing angular velocity on satellite body to track the expected attitude signal. In the satellite attitude control subsystem, there are three control loops from inner the BLDCM to the outer CubeSat: (1) the current loop of the actuator, (2) the angular velocity of the satellite body and (3) the attitude angle loop, which need to be regulated simultaneously. In this article, Matlab-Simulink is applied to construct dynamic mathematical models including the CubeSat body (kinematics, dynamics) module, the three-axis actuator module (BLDCM, reaction wheel), and the active controllers based on the actuator. Specifically, according to the multi-loop control architecture, individual loop controllers are designed through closed-loop system response simulation to complete the coupled cascades interaction between the satellite body and the reaction wheels. Among them, a "P+PI" type control law is proposed, which can achieve precise attitude pointing in terms of time efficiency, stability and robustness as the system control requirements.***

Keywords: Attitude, Attitude Control System(ACS), Low-Earth Orbit(LEO), Electromagnetic(EM) Actuator, Brushless Direct Current Motor(BLDCM), Reaction-wheel, Euler angle, Quaternions

1. Introduction

Nowadays, with the rapid development of aerospace technology and based on the goals of the CubeSat program, satellite payloads with low power consumption, low mass, small size and high reliability are easier to enter the space; moreover, due to the uniform specification of the geometrical structure, the use of The CubeSat standard can also shorten the design and development time. As a result, the number of LEO satellites increases year by year, and they are widely used in telecommunications, weather forecasting, capturing earth images, remote telemetry for environmental scientific research...etc. However, due to different missions and satellite structures with extended solar panels, antennas, cameras, and electromechanical manipulators, space missions have become more and more complex. This complexity leads to mathematical models with nonlinear dynamics which plays an important role in understanding the dynamics and performance of the satellite attitude control system (ACS) [1, 2, 3, 4, 5]. In this article, among the attitude determination control system (ADCS), active actuator using BLDCM with reaction wheel for CubeSat attitude pointing control is explored, and relevant controllers are designed, as shown in Fig.(1) and indicated by the red frame.

1.1 Operational Phases of Satellite Attitude Control

After the satellite is launched into space, it may go through multiple stages of operation, and three attitude control modes may be required in each stage [6]:

De-tumbling mode: Firstly, when the satellite payload reaches the target orbit, after ejecting from the Poly-Picosatellite Orbital Deployer (P-POD) and deploying all the mechanical parts, the satellite may experience a high rolling speed; at this time, the anti-rolling mode is needed to reduce and control the angular rate so as to end the rolling motion of the satellite. Typical methods are B-dot rotation controller and so on.

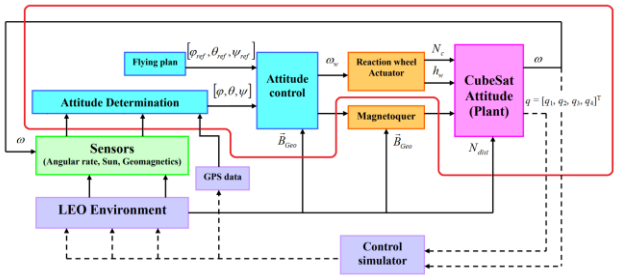

Figure 1: Attitude pointing control actuated by the reaction wheel actuator (red frame)

1) **Three-axes Stabilization mode:** Secondly, after the roll rate of the satellite is reduced and controlled, the three-axes stabilization control mode is applied to make the satellite's attitude as close as possible to a desired direction; ideally, the desired direction is "zero" roll angle (ϕ), pitch angle (θ) and yaw angle (ψ), which means that the axes of the satellite body coordinate (SBC) are aligned with the axes of the orbital reference coordinate (ORC). This is usually achieved by using three-axis magnetorquers devices through interaction with the earth's magnetic field.
2) **Pointing Control mode:** Finally, a satellite that achieves a stable attitude can adopt a directional control mode according to mission requirements, such as: solar panels

track the sun's position for charging, and the camera must be aligned with a specific accuracy of less than 1^{o} RMS Directions to take pictures...etc. Currently, in the ADCS system of CubeSat, reaction wheel and BLDCM are mostly used for active precise attitude control.

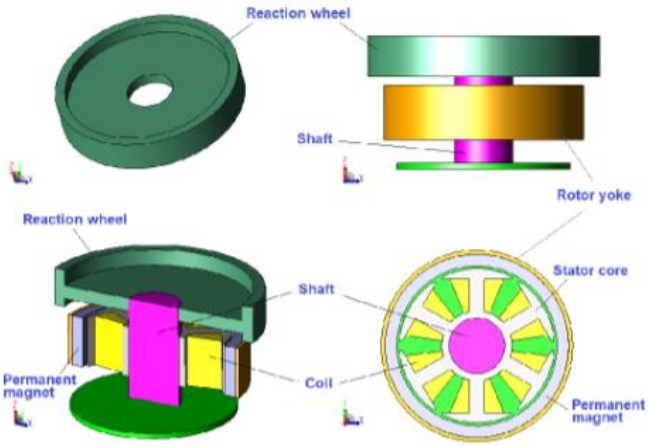

Figure 2: Attitude actuator model of this article: (top left) reaction wheel, (top right) actuator assembly, (bottom left) sectional view of actuator assembly, (bottom right) 3-phase BLDC motor

1.2 EM-Actuator for Attitude Control

The actuator assembly includes an electric motor, which is used to drive a disc or wheel with large mass inertia; and the motor can be integrated in the wheel structure, with permanent magnets (PM) embedded in the periphery of the rotor and a coil is provided on the stator. In this article, a 3U CubeSat uses a BLDCM connected with a reaction-wheel as an actuator, as shown in Fig.(2), which generates control torque imposing angular velocity on satellite body to track the expected attitude signal. CubeSat attitude determination system (ADS) usually processes satellite orientation data through sensors (stellar sensors, magnetometers,…etc.) to form an estimate of satellite attitude, and compares it with the attitude expected by the ACS. If there is an error between the two, the control system generates a corresponding control signal to compensate for the difference. On the other hand, CubeSat uses a combination set of reaction wheels to control the pointing attitude. This is a momentum exchange device that can provide a smooth torque change, so that the satellite's attitude pointing can be accurately achieved through Newton's "Action-reaction" law of motion.

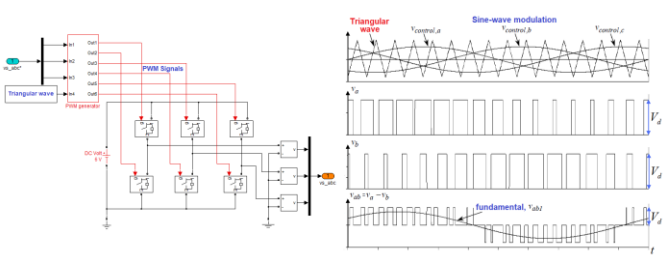

Figure 3: Modular control of the inverter: (left) PWM inverter of PMSM, (right) 3-phase sinusoidal SPWM signal

The first principle of motor control is to gain torque in order to obtain the necessary speed. In this article, the reaction wheels of the CubeSat actuator are driven by the servo control system of the motor, in which the power drive adopts a voltage source inverter (VSI) with sine-wave pulse width modulation (SPWM), as shown in Fig.(3). On the other hand, the speed regulation is implemented according to the scheme of "field-oriented control (FOC)" combined with the constant torque angle (CTA, i.e. i_d = 0) method, as shown in Fig.(4). Therefore, in the process of generating torque, since the current tends to be proportional to the torque ($T_e \cong k_e \cdot i$), the electronic power driver will transfer the necessary current to the motor to implement the torque required by the command. Further, based on the multi-loop architecture of "internal current loop/external speed loop," PI-type controller is used for current and speed controllers to establish control law, please refer to Section (C). [10, 11]

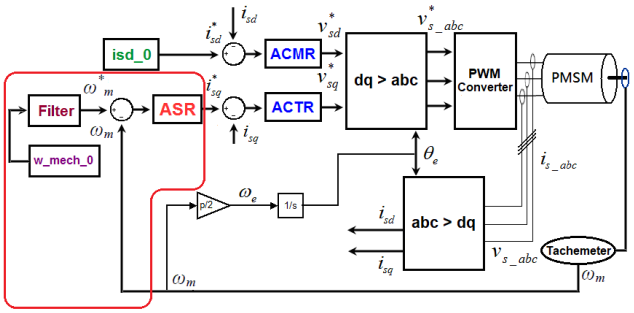

Figure 4: PMSM variable frequency vector control closed loop servo speed regulation system

1.3 Cascaded Multi-Loop of Attitude Control

In the CubeSat attitude control subsystem based on the EM-actuator: the current/speed control of the motor is the inner cascade (as shown in Fig.(5)), and the satellite body angular velocity/attitude is the outer cascade (as shown in Fig. (6)). Among them, there are three control loops: (1) the current of the motor, (2) the speed of the motor and the angular velocity of the satellite body being an overlap of consequence, and (3) the attitude angle of the satellite body. They need to be regulated simultaneously so the motor responds instantly in gaining effective torque and the satellite react spontaneously in pointing accurate attitude. Therefore, in this paper, due mainly to advantageous intrinsic decoupling effect [11], the ACS adopts a multi-loop architecture to accomplish the attitude, speed, and current controls in a hierarchical manner.

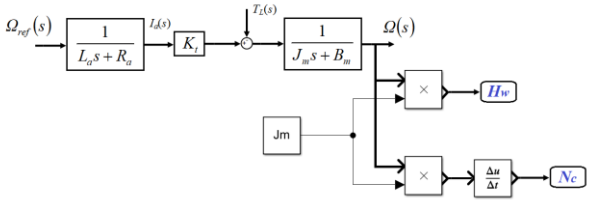

Figure 5: Inner-loop cascade of CubeSat ACS--open-loop of BLDCM and reaction wheel assembly

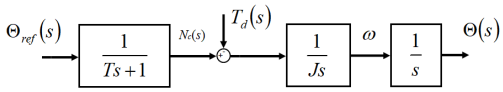

Figure 6: Outer-loop cascade of CubeSat ACS--open-loop of actuator and satellite body

From Fig.(5) and (6), it is obviously that the current is input to the BLDCM in accordance with the attitude command (Θ_{ref}), which initiates the motor speed (Ω) in the inner cascade; in turn, the satellite body in the outer cascade reacts with an angular velocity (ω) through angular momentum exchange between the two counterparts during attitude pointing. This forms a closed loop of speed servo control, in which the reaction wheel outputs the control torque (N_c) and momentum (H_w) as shown on the right side of Fig.(5). Further, the dynamic relationship from the relevant speed control loops to the torque (N_c, N_w) exchange between reaction wheel and satellite body can be derived as follows:

$$\begin{cases} \tau_w \ddot{h} = N_c + N_w \\ N_c = -\dot{h} \end{cases} \quad (1)$$

$$\frac{N_c(s)}{N_w(s)} = \frac{1}{\tau_w s + 1} \quad (2)$$

τ_w: time constant in $\dot{h}$ loop
$\dot{h}$: angular momentum exchange between reaction wheel and satellite body
N_c: control torque of actuator
N_w: torque of satellite body

Taking the Laplace transformation of Eq.(1), the torque transfer function of the reaction wheel acting on the satellite body can be obtained as shown in Eq.(2); and, through Newton's 3rd law of motion, there is a low-pass characteristics from the reaction wheel to the satellite body, and the bandwidth of the relevant speed control is equal to f_n (= $1/\tau_w$); or, specifically: there is a $T = \tau_w$ time delay of torque transmission from the actuator to the satellite body [7, 8]. Therefore, by deriving the reduced model of the combined BLDCM and wheel assembly with speed control, the actuator model in Fig.(6) can be replaced with the transfer function of Eq.(2); in the following, the decoupled satellite cascade can be used independently for control law development and parameter design in attitude pointing control, please refer to section (E).

1.4 Content Organization

In designing the attitude control system, it is important to construct an accurate model to represent the dynamics and kinematics, so as to perform algorithm verification and performance validation [8, 9]. This article is organized according to the following sequence: in section (B), the mathematical model of BLDCM electromagnetic (EM) nonlinearity is derived according to decoupling in the magnetic circuit and d-q dynamic equivalent circuit. In section (C), the PI-type controller is used and the control law and parameter design are carried out based on the architecture of "internal current loop/external speed loop". In section (D), the nonlinear mathematical model of the CubeSat is derived based on the attitude kinematics, dynamics and consideration of quaternion. In section (E), according to the "internal angular velocity loop/external attitude angle loop" structure, the attitude control law and parameter design are implemented for the satellite body cascade. In addition, in sections (B) and (D), the dynamic models of the BLDCM actuator and the satellite subsystem generated by MATLAB/Simulink are introduced respectively. In section (F), the attitude control simulation results are collected to verify the validity and feasibility of the model; also, in section (G), conclusions of this article are made based on comparison among three simulation scenario, and future works are proposed.

2. The PMSM Mathematical Model

In this paper, a three-phase BLDCM combined with a reaction wheel is used to perform active satellite attitude control. As shown in Fig.(2), it is a four-pole, outer rotor permanent magnet synchronous motor (PMSM). This section will derive the dynamic mathematical model of the motor according to the "field orient control (FOC)" scheme with the method of $i_d = 0$, and build-up the Simulink model.

2.1 Hypothesis of Motor Governing Equations

Developing an accurate system model is the primary goal of all motors in respective stages of its design, analysis and control; however, in terms of motor governing equations, the accuracy requirement is different for each stage. In this paper, for rapid modeling purpose, a simplified BLDCM model according to the dynamic voltage equation (Eq.(3)) follows assumptions listed below [10, 11]:

- Obtain the lumped parameters of constant inductance (L_d, L_q) by ignoring the non-linearity (geometry, material) in the magnetic circuit and omitting the stator flux leakage of the PMSM.
- Obtain a constant phase resistance (R_s) of stator coil by ignoring the variation of temperature, and measuring DC current at room temperature.
- Calculate the electromagnetic torque by ignoring the motor (copper/iron) losses, and based on the equality between electromagnetic input power and mechanical output power.

$$v_a(t) = R_a i_a(t) + L_a \frac{di_a(t)}{dt} + K_{emf}\omega(t) \quad (3)$$

where, v_a is armature voltage, R_a is armature resistance, i_a is armature current, ω is rotor speed, K_{emf} is back electromotive force constant; and $K_{emf}\omega(t)$ (= $e_g(t)$) is the back electromotive force of the motor.

2.2 PMSM Dynamic Mathematical Model

PMSM can operate with frequency conversion and speed regulation, because it includes electronic drive and servo control systems. However, due to Faraday's law, the flux linkage between PMSM rotor and stator not only is coupled, but also changes continuously along with the rotor positions.

This EM nonlinearity induces complex dynamic properties. Therefore, if it is to carry out a similar driving and control scheme equivalent to the DC motor, the relevant governing equation system must be decoupled in the magnetic circuit. Mathematically, this can be achieved by converting the three-phase AC winding (3s) into a set of mutually independent and orthogonal two-phase DC windings (2r) in the synchronous rotating coordinate system. Specifically, as shown in the left picture of Fig.(7), the three-phase dynamic model of the motor is transformed into a static two-phase orthogonal model by Clark transformation, which achieves the decoupling of the physical variables of each phase; on the other hand, as shown in the right picture of Fig.(7), it is further transformed into a synchronously rotating two-phase orthogonal model after Park transformation, which makes the physical variable become a time-invariant DC value.

The PMSM model mentioned above comply with the basic characteristic that the steady-state speed of the motor is always equal to the synchronous speed. And, assumes that the positive direction of the d-axis corresponds to the N-pole of the permanent magnet on the rotor, a set of voltage and flux linkage equations as shown in Eq.(4)~(8) can be derived using Park transformation. Then, the associated dynamic equivalent circuit of PMSM in the d-q reference coordinate system can be obtained, as shown in Fig.(8).

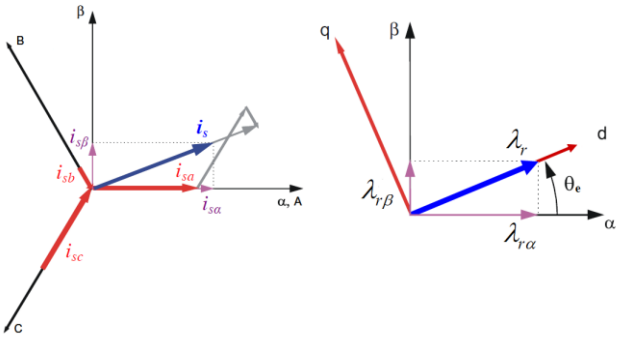

Figure 7: Coordinate transformations of PMSM: (left) Clark transformation, (right) Park transformation

$$v_d = R_s i_d + \frac{d\lambda_d}{dt} - \omega_e \lambda_q \quad (4)$$

$$v_q = R_s i_q + \frac{d\lambda_q}{dt} + \omega_e \lambda_d \quad (5)$$

$$\lambda_d = L_d i_d + \lambda_{pm} \quad (6)$$

$$\lambda_q = L_q i_q \quad (7)$$

$$\omega_e = n_p \cdot \omega_m \quad (8)$$

λ_d, λ_q : d-q flux linkage
L_d, L_q : d-q inductance
λ_{pm} :PM flux linkage
ω_e : EM angular velocity
ω_m : rotor mechanical velocity
n_p : pole pair number

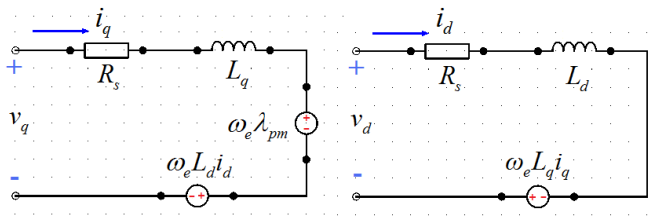

Figure 8: PMSM dynamic equivalent circuit model in d-q reference coordinate system

Furthermore, based on the assumptions listed above, the time-varying terms in the voltage equations (such as Eqs.(4) and (5)) of PMSM are deleted under the steady-state condition of constant speed, and a set of reduced mathematical algebraic expression is obtained:

$$v_d = -\omega_e L_q i_q \quad (9)$$

$$v_q = \omega_e \left(L_d i_d + \lambda_{pm}\right) \quad (10)$$

$$\hat{I}_s = \sqrt{i_d^2 + i_q^2} \quad (11)$$

$$\hat{V}_s = \sqrt{v_d^2 + v_q^2} \quad (12)$$

$\hat{I}_s$: magnitude of current vector
$\hat{V}_s$: magnitude of voltage vector

Firstly, under the principle of constant power, the input power of the motor can be expressed as follow:

$$P_{in} = \begin{bmatrix} v_a & v_b & v_c \end{bmatrix} \cdot \begin{bmatrix} i_a \\ i_b \\ i_c \end{bmatrix} = \frac{3}{2} \cdot \begin{bmatrix} v_d & v_q \end{bmatrix} \cdot \begin{bmatrix} i_d \\ i_q \end{bmatrix} \quad (13)$$

And, based the assumption of no motor losses, as well as from Eqs.(8), (9) and (10), the relationship of equal input and output powers ($P_{in} = P_{out}$):

$$P_{out} = \frac{3}{2} \cdot \left(v_d i_d + v_q i_q\right) = \frac{3}{2} \cdot \omega_e \left[\lambda_{pm} i_q + \left(L_d - L_q\right) i_d i_q\right] = \frac{3}{2} \cdot n_p \cdot \omega_m \left[\lambda_{pm} i_q + \left(L_d - L_q\right) i_d i_q\right] \quad (14)$$

Therefore, the output torque of the PMSM motor can be expressed as follow:

$$T_{em} = \frac{P_{out}}{\omega_m} = \frac{3}{2} \cdot n_p \cdot \left[\lambda_{pm} i_q + \left(L_d - L_q\right) i_d i_q\right] \quad (15)$$

Also, considering the load torque, friction torque) and motor's moment of inertia, and according to Newton's second law of motion, the electromechanical equation of the motor is derived as follow:

$$T_{em} - T_L = J \frac{d\omega_m}{dt} + B\omega_m \quad (16)$$

T_L : load torque
B : friction coefficient
J : equivalent MI. of motor rotor and reaction wheel

PMSM's mathematical model is usually established in the rotor reference frame (i.e. the d-q coordinate system), and the governing equations can be summarized as listed in Table(1):

Table 1: Governing equations of PMSM

Electromagnetic Torque Equation:	
$T_{em} = \frac{3}{2} \cdot n_p \cdot \left[\lambda_{pm} i_q + \left(L_d - L_q\right) i_d i_q\right]$	(15)
Equation of Motion:	
$T_{em} - T_L = J \frac{d\omega_m}{dt} + B\omega_m$	(16)
Voltage Equations:	
$v_d = R_s i_d + L_d \frac{di_d}{dt} - \omega_e L_q i_q$	(4 & 9)
$v_q = R_s i_q + L_q \frac{di_q}{dt} + \omega_e \left(L_d i_d + \lambda_{pm}\right)$	(5 & 10)

2.3 Simulink Modeling of PMSM

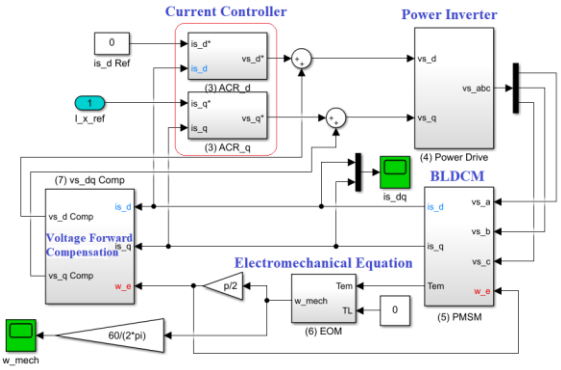

Figure 9: BLDCM dynamic Simulink model

As shown in Fig.(9), according to governing equations listed in Table(1), the three-phase BLDC motor of this paper is constructed into Simulink block diagram and form a d-q synchronous rotation system model, which includes: current controller block diagrams, voltage source inverter (VSI) using sine-wave pulse width modulation (SPWM) (as shown in Fig.(3)), the motor body (as shown in Fig.(10)), and the motor's equation of motion block diagram (as shown in Fig.(11)).

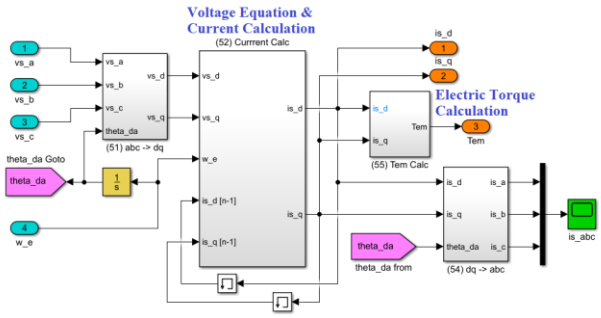

Figure 10: BLDC motor body block diagram

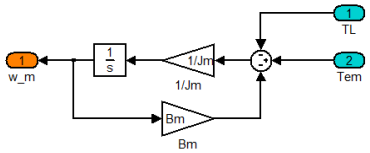

Figure 11: Motor's equation of motion block diagram

As shown in Fig.(10), in addition to the coordinate transformation blocks such as 'abc->dq' and 'dq->abc', the motor body mainly contains the current calculation block based on the flux linkage and voltage equations (see Fig.(12)), as well as an electromagnetic torque (T_e) calculation block.

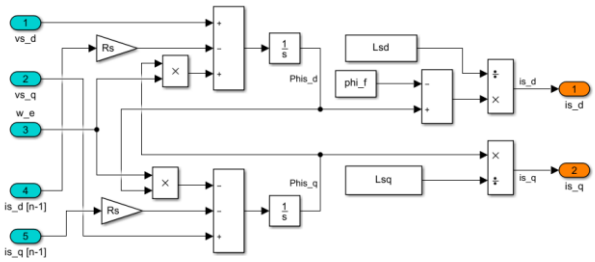

Figure 12: PMSM current calculation block diagram

3. BLDCM Controllers

In order to simplify the derivation process of the control law of the actuator and the satellite, as well as the subsequent construction of the respective dynamic models, this paper ignores the sensors in each of the control loops, and adopts the deterministic unit negative feedback for simulation and analysis. [10, 11, 12]

3.1 BLDCM Current Controller (ACR)

Generally, PMSM uses two controllers to regulate the current and speed simultaneously. And according to a typical two-layer closed-loop servo control system as shown in Fig.(4), the current controller is designed prior to the speed counterpart. In this paper, PI-type regulator is applied for regulating the motor performance, because the proportional control can ensure the stability of the system, and the integrator can achieve no static error. Moreover, under the assumption that the characteristic frequency (ω_{ref}) of the speed loop is much smaller than that (ω_c) of the current loop, that is, $\omega_{ref} << \omega_c$, the parameter regulation rules of the respective controllers are developed:

1) Current controller (ACR): To achieve the ideal current control, the current closed-loop transfer function is approximately "1" ($G_{ACR\_close}(s) \approx 1$).
2) Speed controller (ASR): Combined with the speed filter ($G_f(s)$), the speed closed-loop transfer function ($G_{ASR\_close}(s)$) forms a standard second-order system to facilitate the use of undamped natural frequency (ω_n) and damping ratio (ζ) to develop the parameters of the controller.

Moreover, without affecting the simulation results, assumptions are taken to simplify the derivation process: (1) The current and speed closed-loops have no disturbance terms $T_L = 0$, $E_g = 0$; and (2) The mechanical time constant is much greater than the electrical time constant (i.e., $\tau_M >> \tau_E$).

According to equations (3) and (16) and under zero initial conditions, the dynamic mathematical equations after Laplace transformation are as follows:

$$I_a(s) = \frac{1}{L_a s + R_a}[V_a(s) - K_{emf}\Omega(s)] \quad (17)$$

$$\Omega(s) = \frac{1}{J_m s + B_m}[K_t I_a(s) - T_L(s)] \tag{18}$$

where, $V_a(s)$, $I_a(s)$, $T_L(s)$, $\Omega(s)$ are the Laplace transformations of $v_a(t)$, $i_a(t)$, $\tau_L(t)$, $\omega(t)$, respectively. In addition, the relevant open loop of the actuator subsystem is shown in Fig.(5).

To simplify the derivation of the transfer function for the current controller, the back EMF ($e_g(t)$) in the voltage equation (Eq.(3)) is set as an independent armature voltage compensation, so as to combine with a linear first-order voltage $v_a^*(t)$ and formulate as $v_a(t) = v_a^*(t) + e_g(t)$, where $v_a^*(t) = R_a i_a(t) + L_a \frac{di_a(t)}{dt}$. In this way, the current closed-loop of the BLDCM model can be transformed as shown in the left block diagram of Fig.(12); at the same time, the current transfer function serving as a controlled plant correspondingly becomes as Eq.(19):

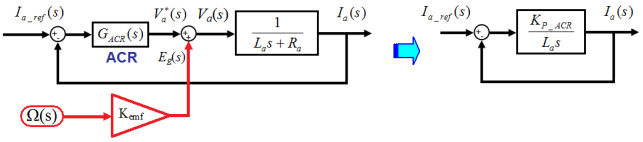

Figure 12: BLDCM armature voltage compensation associated in the current closed-loop

$$\frac{I_a(s)}{V_a^*(s)} = \frac{1}{L_a s + R_a} \tag{19}$$

$$G_{ACR}(s) = K_{P\_ACR}\left(1 + \frac{K_{I\_ACR}}{K_{p\_ACR} s}\right) = K_{P\_ACR}\left(1 + \frac{1}{T_{I\_ACR} s}\right) \tag{20}$$

Take the PI-type current controller ($G_{ACR}(s)$) as Eq.(20), and set the integral time constant of current control equal to the electrical time constant, that is, $T_{I\_ACR} = \tau_E = (L_a/R_a)$; then the simplified current open-loop transfer function is as Eq.(21), and the current closed-loop becomes as shown on the right of Fig.(12), and the corresponding closed-loop transfer function is as Eq.(22):

$$G_{ACR\_open}(s) = \frac{K_{P\_ACR}}{L_a} \tag{21}$$

$$G_{ACR\_close}(s) = \frac{\frac{K_{P\_ACR}}{L_a}}{s + \frac{K_{P\_ACR}}{L_a}} = \frac{\omega_c}{s + \omega_c} \tag{22}$$

Now, if the characteristic frequency of the current loop is set $\omega_c = (K_{P\_ACR}/L_a)$, such that $G_{ACR\_close}(s) = 1$ to achieve ideal current control, then the parameters of the current controller can be designed according to the following regulation rules:

$$K_{P\_ACR} = L_a \omega_c \tag{23}$$

$$K_{I\_ACR} = R_a \omega_c \tag{24}$$

3.2 BLDCM Speed Controller (ASR)

In designing the speed controller, under the assumption of $\omega_{ref} << \omega_c$, the speed control block diagram based on the scheme depicted in Fig.(13) consists of the ideal controlled current block, the speed controller ($G_{ASR}(s)$) and the speed filter ($G_f(s)$). As can be seen, the current closed-loop transfer function of Eq.(22) shown in Fig.(12) is applied, and the relevant $G_{ASR}(s)$ and $G_f(s)$ transfer functions are shown as Eqs.(25) and (26).

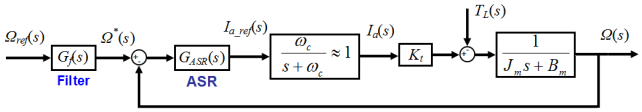

Figure 13: The speed control block diagram after adding speed controller ($G_{ASR}(s)$) and filter ($G_f(s)$).

$$G_{ASR}(s) = K_{p\_ASR}\left(1 + \frac{K_{I\_ASR}}{K_{P\_ASR} s}\right) = K_{P\_ASR}\left(1 + \frac{1}{T_{I\_ASR} s}\right) \tag{25}$$

$$G_f(s) = \frac{K_{I\_ASR}}{K_{P\_ASR} s + K_{I\_ASR}} = \frac{1}{T_{I\_ASR} s + 1} \tag{26}$$

According to Fig.(13), under the assumption of $T_L = 0$, the speed closed-loop transfer function can be derived as in Eq.(27); among them, the setup of filter ($G_f(s)$) can eliminate the zero of numerator in Eq.(27) and make $G_{ASR\_close}(s)$ a standard second-order system which is suitable for setting the regulation law of the speed controller parameters as shown in Eqs. (28) and (29):

$$G_{ASR\_close}(s) = \frac{\frac{K_{P\_ASR}}{J_m}\left(s + \frac{K_{I\_ASR}}{K_{P\_ASR}}\right)}{s^2 + \left(\frac{1}{\tau_M} + \frac{K_{P\_ASR}}{J_m}\right)s + \frac{K_{I\_ASR}}{J_m}} = \frac{\omega_n^2}{s^2 + 2\omega_n \zeta s + \omega_n^2} \tag{27}$$

$$K_{P\_ASR} = J_m\left(2\omega_n \zeta - \frac{1}{\tau_M}\right) \tag{28}$$

$$K_{I\_ASR} = J_m \omega_n^2 \tag{29}$$

4. The Satellite Attitude Mathematical Model

The rotation of the satellite can be described by Euler equations of kinematics and dynamics; the former specifies the time evolution of satellite attitude parameters, while the latter considers the effect of torque applied on the rate changes of the satellite angular velocity vector. And, in this article, the behavior of the reaction wheel to the satellite can be confirmed by developing a dynamic model as shown in Fig.(14). Among them, the input includes: the torque (N_w) and angular momentum (h_w) of the reaction wheel, as well as external disturbance torque (N_e, such as gravity gradient, aerodynamic

drag, solar radiation pressure...etc.); and the relevant output includes: the angular momentum (H) and angular velocity (ω) of the satellite body, as well as the attitude in the quaternion format [3, 7, 8]. In this article, it is assumed that the satellite is a rigid body and its mass does not change (i.e. J_s is a constant value), and the three sets of electromagnetic actuator are organized to respectively align with the three orthogonal axes of the principal-axis frame. In addition, the control torque (N_c) in terms of the reaction wheel is much larger than those disturbance (N_e) from the LEO environment, and only the gravity gradient torque (T_{gg}) is included in the satellite dynamic model.

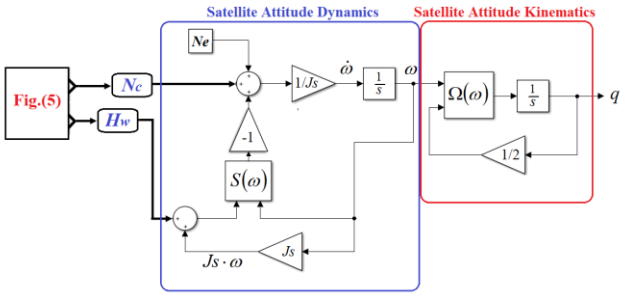

Figure 14: Satellite's nonlinear model of dynamics and kinematics

4.1 Satellite Attitude Dynamics Mathematical Model

According to the Euler equation of rotation dynamics as shown in Eq.(30): the change of the satellite angular rate is based on the total torque ($\vec{N}_{tot}$) acting on the satellite being equal to the sum of the external torque (determined by the environmental fields), and it can be derived to describe the satellite movement relative to the inertial reference coordinates. In addition, the dynamics equation can be expressed in vector form as $\dot{\vec{H}}_{tot} = \vec{N}_e - \vec{\omega} \times \vec{H}_{tot}$ in terms of the satellite body coordinate, and its specific physical meaning: the rotation motion (i.e., angular momentum, $\vec{H}_{tot} = J_s \cdot \vec{\omega} + \vec{h}_w$) of the satellite body (including the reaction wheel) will continue unless being changed by torque (such as $\dot{\vec{h}}_w$ from reaction wheel).

$$\frac{d}{dt}(J_s\vec{\omega}) + \dot{\vec{h}}_w = \vec{N}_e - \vec{\omega} \times J_s\vec{\omega} - \vec{\omega} \times \vec{h}_w \tag{30}$$

$$\dot{\vec{\omega}} = \left(-J_s^{-1}\right)\left[S(\omega)J_s\vec{\omega} - S(\omega)\vec{h}_w + \vec{N}_c + \vec{N}_e\right] \tag{31}$$

where $S(\omega)$ is the product operator:

$$S(\omega) = \begin{bmatrix} 0 & -\omega_3 & \omega_2 \\ \omega_3 & 0 & -\omega_1 \\ -\omega_2 & \omega_1 & 0 \end{bmatrix}$$

As shown on the left of Fig.(14), the basic items of satellite dynamics include: satellite moment of inertia (J_s), satellite angular velocity (ω), reaction wheel angular momentum (h_w), external torque (N_e), and the control torque (N_c) from the reaction wheel that causes the total angular momentum to change; and, these are physical quantities of the satellite body coordinate [7, 8]. Moreover, the satellite attitude dynamics equation is completed by determining the control torque ($\dot{\vec{h}}_w = -\vec{N}_c$) of the reaction wheel, as shown in Eq.(31).

Therefore, substituting the x-, y-, z- components of J_s, ω, h_w into Eq.(31), the satellite angular acceleration ($\dot{\omega}$) in three axes format as expressed in Eq.(32) is obtained, which leads into the kinematical operation as shown in the red frame on the right side of Fig.(14):

$$\begin{bmatrix} \dot{\omega}_x \\ \dot{\omega}_y \\ \dot{\omega}_z \end{bmatrix} = \begin{bmatrix} \left[N_{gyro\_x} + N_{c\_x} + N_{e\_x}\right] I_{xx}^{-1} \\ \left[N_{gyro\_y} + N_{c\_y} + N_{e\_y}\right] I_{yy}^{-1} \\ \left[N_{gyro\_z} + N_{c\_z} + N_{e\_z}\right] I_{zz}^{-1} \end{bmatrix} \tag{32}$$

$$\vec{N}_{gyro} = S(\omega)J_s\vec{\omega} - S(\omega)\vec{h}_w \tag{33}$$

where, $\dot{\omega}_x, \dot{\omega}_y, \dot{\omega}_z$ are satellite angular accelerations, N_{gyro} is gyro torque of angular momentum exchange, and I^{-1}_{xx}, I^{-1}_{yy}, I^{-1}_{zz} are the inverse of satellite MI. (I^{-1}_s) in the three axes components.

4.2 Satellite Attitude Kinematics Mathematical Model

In analyzing and designing the attitude control system, it is important to define the reference coordinate system. Specifically, deviation of the attitude due to satellite rotational movement can be described according to the relativity between satellite body frame (F_b) and orbit reference frame (F_o). In addition, the rotation matrix is usually applied to calculate the direction of F_b relative to F_o, which is useful for pointing the satellite to a specific target (such as the earth) and for defining the orientation. On the other hand, any rotational motion can be described in terms of a series of three-axis rotation angles; in other words, the Euler rotation sequence. In this article, the satellite attitude kinematics equation is derived in accordance with the "Euler 3-2-1 rotation sequence", i.e., z-axis yaw angle (ψ) => y-axis pitch angle (θ) => x-axis roll angle (ϕ), which is applied to construct the Simulink model [3, 7, 9].

Euler angle and unit quaternion are often used to indicate the attitude of satellites in reference coordinates; and, due to the consideration of the singularity in Euler angle, the unit quaternion will be used in the simulation. The definition of unit quaternion is as in Eq.(34), which is used to express a unit vector (e_x, e_y, e_z) rotated by an angle of α; moreover, it can be expressed as: $q = [q_1, q_2, q_3, q_4]^T$ and $q_1^2 + q_2^2 + q_3^2 + q_4^2 = 1$, where q_1, q_2, q_3 describe the coordinates of the Euler axis in 3D space, and q_4 is a constant between [-1, 1] and describes the amplitude of the rotation angle [14, 15].

$$\begin{bmatrix} q_1 \\ q_2 \\ q_3 \end{bmatrix} = \begin{bmatrix} e_x \sin\left(\frac{\alpha}{2}\right) \\ e_y \sin\left(\frac{\alpha}{2}\right) \\ e_z \sin\left(\frac{\alpha}{2}\right) \end{bmatrix}, \quad q_4 = \cos\sin\left(\frac{\alpha}{2}\right) \tag{34}$$

In addition, based on "Euler 3-2-1 rotation sequence," the formulas for converting between Euler angle and unit quaternion are as shown in Eqs.(35) and (36), respectively:

$$\begin{bmatrix} q_1 \\ q_2 \\ q_3 \\ q_4 \end{bmatrix} = \begin{bmatrix} \sin\left(\frac{\phi}{2}\right)\cos\left(\frac{\theta}{2}\right)\cos\left(\frac{\psi}{2}\right) - \cos\left(\frac{\phi}{2}\right)\sin\left(\frac{\theta}{2}\right)\sin\left(\frac{\psi}{2}\right) \\ \cos\left(\frac{\phi}{2}\right)\sin\left(\frac{\theta}{2}\right)\cos\left(\frac{\psi}{2}\right) + \sin\left(\frac{\phi}{2}\right)\cos\left(\frac{\theta}{2}\right)\sin\left(\frac{\psi}{2}\right) \\ \cos\left(\frac{\phi}{2}\right)\cos\left(\frac{\theta}{2}\right)\sin\left(\frac{\psi}{2}\right) - \sin\left(\frac{\phi}{2}\right)\sin\left(\frac{\theta}{2}\right)\cos\left(\frac{\psi}{2}\right) \\ \cos\left(\frac{\phi}{2}\right)\cos\left(\frac{\theta}{2}\right)\cos\left(\frac{\psi}{2}\right) + ain\left(\frac{\phi}{2}\right)\sin\left(\frac{\theta}{2}\right)\sin\left(\frac{\psi}{2}\right) \end{bmatrix} \quad (35)$$

$$\begin{bmatrix} \phi \\ \theta \\ \psi \end{bmatrix} = \begin{bmatrix} \text{atan}\left(\frac{2(q_1q_4 + q_2q_3)}{q_3^2 + q_4^2 - q_1^2 - q_2^2}\right) \\ \text{asin}(2(q_2q_4 - q_1q_3)) \\ \text{atan}\left(\frac{2(q_3q_4 + q_1q_2)}{q_1^2 + q_4^2 - q_2^2 - q_3^2}\right) \end{bmatrix} \quad (36)$$

Therefore, as shown in Fig.(14), the satellite angular acceleration ($\dot{\omega}$, as in Eq.(32)) can be calculated by using the Euler angle and unit quaternion converting formula; in this way, in terms of the unit quaternion $[q_1, q_2, q_3, q_4]^T$, the satellite attitude kinematics can be derived as follows according to the angular velocity (ω):

$$\dot{q} = \frac{1}{2}\Omega(\omega)q = \frac{1}{2}\begin{bmatrix} 0 & \omega_3 & -\omega_2 & \omega_1 \\ -\omega_3 & 0 & \omega_1 & \omega_2 \\ \omega_2 & -\omega_1 & 0 & \omega_3 \\ -\omega_1 & -\omega_2 & -\omega_3 & 0 \end{bmatrix} q \quad (37)$$

Or, by separating the scalar part (q_4) in the quaternion vector from the other three quaternion elements, which define the Gibbs vector with g = (q_1, q_2, q_3), the equation of motion according to the Gibbs vector can be revised as follows:

$$\begin{cases} \dot{g} = -\frac{1}{2}S(\omega)g + \frac{1}{2}q_4\omega; \\ \dot{q}_4 = -\frac{1}{2}\omega^T g \end{cases} \Rightarrow \begin{bmatrix} \dot{g} \\ \dot{q}_4 \end{bmatrix} = \frac{1}{2}\begin{bmatrix} -S(\omega) \\ -\omega^T \end{bmatrix} g + \frac{1}{2}q_4\begin{bmatrix} I_{3\times3} \\ 0 \end{bmatrix}\omega \quad (38)$$

Finally, according to Eq.(32) and the expanded Eq.(38) quaternion matrix, the governing equations of satellite attitude dynamics and kinematics can be summarized as shown in Table(2):

Table 2: Governing equations of satellite kinematics and dynamics

Attitude Dynamics Equation:

$$\begin{bmatrix} \dot{\omega}_x \\ \dot{\omega}_y \\ \dot{\omega}_z \end{bmatrix} = \begin{bmatrix} \left[N_{gyro\_x} + N_{c\_x} + N_{e\_x}\right]I_{xx}^{-1} \\ \left[N_{gyro\_y} + N_{c\_y} + N_{e\_y}\right]I_{yy}^{-1} \\ \left[N_{gyro\_z} + N_{c\_z} + N_{e\_z}\right]I_{zz}^{-1} \end{bmatrix} \quad (32)$$

Attitude Kinematics Equation:

$$\begin{bmatrix} \dot{q}_1 \\ \dot{q}_2 \\ \dot{q}_3 \\ \dot{q}_4 \end{bmatrix} = \frac{1}{2}\begin{bmatrix} 0 & \omega_3 & -\omega_2 & \omega_1 \\ -\omega_3 & 0 & \omega_1 & \omega_2 \\ \omega_2 & -\omega_1 & 0 & \omega_3 \\ -\omega_1 & -\omega_2 & -\omega_3 & 0 \end{bmatrix}\begin{bmatrix} q_1 \\ q_2 \\ q_3 \end{bmatrix} + \frac{1}{2}\begin{bmatrix} q_4 & 0 & 0 & 0 \\ 0 & q_4 & 0 & 0 \\ 0 & 0 & q_4 & 0 \\ 0 & 0 & 0 & 0 \end{bmatrix}\begin{bmatrix} \omega_1 \\ \omega_2 \\ \omega_3 \end{bmatrix} \quad (39)$$

4.3 Simulink Modeling of Satellite Attitude Control

The related Simulink block diagram as shown in Fig.(15) is constructed according to the governing equations listed in Table(2), which includes: attitude and angular velocity controller block, EM actuator block (as shown in Fig.(16)), attitude dynamics block (as shown in Fig.(17)) and attitude kinematics block (as shown in Fig.(18)).

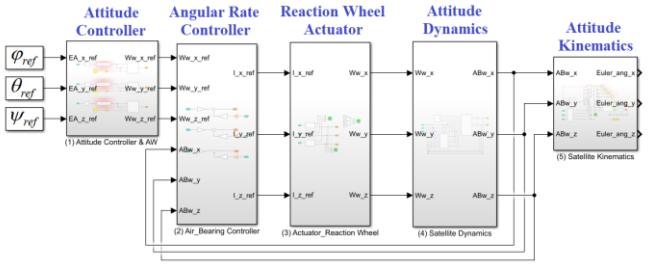

Figure 15: Satellite attitude dynamic control Simulink model

In Fig.(16), three BLDCMs as shown in Fig.(9) are integrated in the actuator assembly block to receive the synthetic current signals from the attitude controller and the angular velocity controller; and, which respectively generate the control torque (N_c) in satellite's three axes. As shown in Fig.(17), the attitude dynamics block includes: gravity gradient torque calculation block, gyro torque calculation block, and satellite angular acceleration calculation block according to Eq.(32).

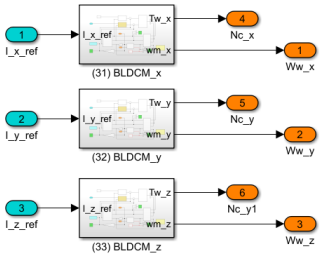

Figure 16: EM actuator assembly with three BLDCMs

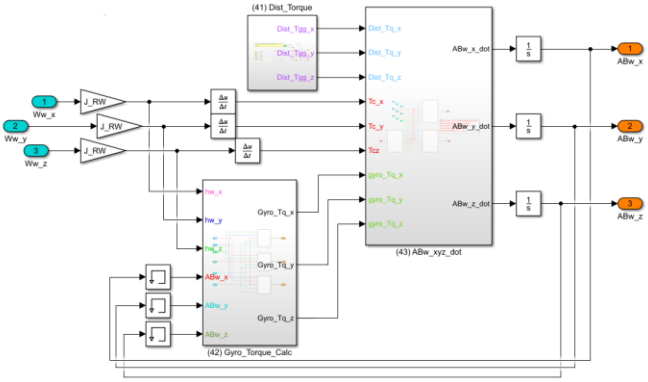

Figure 17: Satellite attitude dynamics model

As shown in Fig.(18), the attitude kinematics block includes: the block for calculating quaternion in terms of Euler angular velocity according to Eqs.(35) and (39), and the block for calculating Euler angle according to Eq.(36).

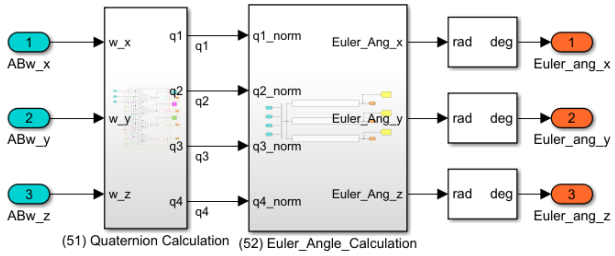

Figure 18: Satellite attitude kinematics model

5. CubeSat Attitude Controllers

As mentioned in section (A-3), it is possible to decouple the two cascades of the satellite body and the actuator assembly, so that satellite attitude control can be indeptmently implemented according to the "internal angular velocity loop/external attitude angle loop" architecture [10, 12]. On the other hand, based on the satellite attitude dynamics model interpreted in section (D-1), the reaction wheel speed (ω_n) and the satellite body angular velocity (ω) rotate in opposite directions along with their angular momentum exchanges due to Newton's "action-reaction" law of motion. Therefore, as a matter of fact, the two velocity loops in Fig.(5) and Fig.(6) are in one dynamic process, but the former is passed to the latter with a τ_w time delay! In other words, as shown in Fig.(4), the reaction wheel speed (ω_n) loop framed in red-line overlaps with that of the satellite body speed (ω), which is omitted in the controller modeling.

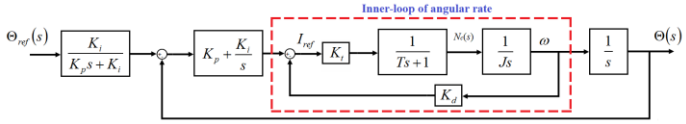

Figure 19: Satellite multi-loop "internal angular rate loop/external attitude angle loop" architecture

However, in this satellite body cascade, the angular velocity and attitude angle loops simultaneously restrain the reference signal (I_{ref}) of the control current to prompt the actuator motor to output torque to synchronously control the angular velocity and attitude orientation of the satellite. Therefore, as shown in Fig.(19), this paper proposes a "P+PI" type control law: (1) the internal angular velocity loop adopts a P-type controller (K_d) which is placed in the negative feedback path of the controlled plant, and (2) the external attitude angle loop applies a PI-type controller (K_p+K_i/s). In addition, under the assumption that the characteristic frequency (ω_n) of the angular velocity loop is much greater than the characteristic frequency (ω_θ) of the attitude loop, that is, $\omega_n >> \omega_\theta$, the parameter regulation rules of the respective controllers are established.

5.1 CubeSat Angular Velocity Controller (SVR)

The angular velocity loop in the multi-loop architecture of the satellite body is shown in the red dashed box in Fig.(19), and its open-loop transfer function ($G_{SVR\_O}(s)$) is as Eq.(40). Moreover, the angular velocity loop can be multiplied by the value of 'K_d' to form a standard second-order system, and the relevant closed-loop transfer function ($G'_{SVR\_C}(s)$) is derived as Eq.(41):

$$G_{SVR\_O}(s)=\frac{\omega(s)}{I_{ref}(s)}=\frac{K_t}{TJs^2+Js} \tag{40}$$

$$G'_{SVR\_C}(s)=K_d\cdot G_{SVR\_C}(s)=\frac{\frac{K_tK_d}{TJ}}{s^2+\frac{1}{T}s+\frac{K_tK_d}{TJ}}\cong\frac{\omega_s^2}{s^2+2\varsigma\omega_s s+\omega_s^2} \tag{41}$$

where, $T=\tau_w$ is time constant of motor speed loop, $\omega_n=2\pi/\tau_w$, ω_s is satellite body angular rate, J is satellite MI. (i.e., J_{xx}, J_{yy}, J_{zz}), K_t is motor torque coefficient, and ζ is damping coefficient.

Now, if the characteristic frequency of the angular velocity ω_s = ($\omega_n/(2\zeta)$) and $\zeta \geqq 1$ are set as the specifications, then the parameters of the angular velocity controller can be defined according to the following regulation rules:

$$K_d=\frac{J\omega_n}{4\varsigma^2K_t} \tag{42}$$

5.2 CubeSat Attitude Angle Controller (SAR)

Similar to the motor speed controller (ASR), under the assumption of $\omega_n >> \omega_\theta$ and the ideal angular velocity control ($G'_{SVR\_O}(s) \approx 1$), the multiple loops architecture of the satellite body (as shown in Fig.(19)) can be simplified as shown in Fig.(20). The related closed-loop transfer function ($G_{SAR\_C}(s)$) is as Eq.(43):

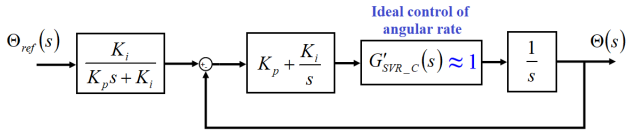

Figure 20: Satellite attitude closed-loop

$$G_{SAR\_C}(s)=\frac{\theta_O(s)}{\theta_{ref}(s)}=\frac{K_ps+K_i}{s^2+K_ps+K_i} \tag{43}$$

Similarly, to make the closed-loop transfer function reveal in the form of a standard second-order system, a filter ($G'_f(s)$) of Eq.(44) is added; and, the relevant closed-loop transfer function ($G'_{SAR\_C}(s)$) is as Eq.(45):

$$G'_f(s)=\frac{K_i}{K_ps+K_i} \tag{44}$$

$$G'_{SAR\_C}(s)=G_{SAR\_C}(s)\cdot\frac{K_i}{K_ps+K_i}=\frac{K_i}{s^2+K_ps+K_i}\cong\frac{\omega_\theta^2}{s^2+2\varsigma_\theta\omega_\theta s+\omega_\theta^2} \tag{45}$$

At this time, if the characteristic frequency (ω_θ) and damping coefficient (ζ_θ) of the attitude angle controller are used as specifications, the relevant parameters can be established according to the following regulation rules:

$$K_p = 2\omega_\theta \zeta_\theta \quad (46)$$

$$K_i = \omega_\theta^2 \quad (47)$$

6. Attitude Control Simulation and Analysis

Table 3: Conditions for dynamic simulation of attitude control

Case	Initial Condition	Value	Reference Attitude
I	$[\varphi_0, \theta_0, \psi_0]$	[0º, 0º, 0º]	[15º, -15º, 15º]
	$[\omega_{x0}, \omega_{y0}, \omega_{z0}]$	[0, 0, 0]	
II	$[\varphi_0, \theta_0, \psi_0]$	[0º, 0º, 0º]	[15º, -7º, 5º]
	$[\omega_{x0}, \omega_{y0}, \omega_{z0}]$	[-0.1, 0.1, -0.1]	
III	$[\varphi_0, \theta_0, \psi_0]$	[0º, 0º, 0º]	[15º, -7º, 5º]
	$[\omega_{x0}, \omega_{y0}, \omega_{z0}]$	[-0.15, 0.12, -0.1]	

This section simulates and analyzes the attitude control of the CubeSat dynamic model according to the conditions listed in Table (3). The relevant specification data and system parameters of BLDCM, CubeSat and controllers respectively, are attached in ANNEX for reference; moreover, the necessary data items are made into (*.m) format files and pre-loaded into MATLAB/Simulink environment for simulation.

6.1 Case (I) Attitude Control Analysis

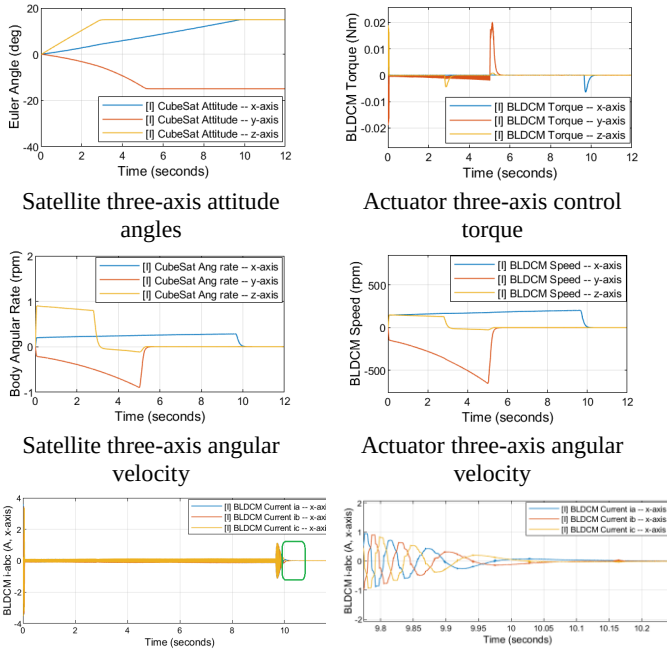

Satellite three-axis attitude angles

Actuator three-axis control torque

Satellite three-axis angular velocity

Actuator three-axis angular velocity

BLDCM three-phase current (i_a, i_b, i_c): (left) full-range, (right) steady state

Figure 21: CubeSat attitude control simulation output results based on Case [I] scenario

Case [I] is to simulate a scenario of starting the CubeSat body from stationary with attitude of [φ_0 = 0º, θ_0 = 0º, ψ_0 = 0º], and then driven by the reaction wheel motor to the reference attitude [15º, -15º, 15º]. From the relevant waveforms of the output results shown in Fig.(21), it is clear that: (1) Since the "Euler 3-2-1 rotation sequence" is adopted in the kinematics model, no matter how the attitude or angular rate changes, all three axes of the vehicle follow the sequence of "z-axis => y-axis => x-axis" to complete the reference tracking process, and achieve an error-free attitude control, as shown in the attitude angle output waveform in Fig.(21).

In addition, (2) The output waveforms of three-axis dynamic angular velocities between satellite body and the three reaction wheel motors are similar: Firstly, during the starting transient process, according to the satellite attitude dynamics model, the torque (N_c) of the BLDCM actuates the reaction wheel and the satellite body to rotate in opposite directions and carry out angular momentum exchange; and, their angular velocities differentiate due to the different magnitudes of the moment of inertia between the two. Afterwards, as the x-axis completes the attitude tracking and the system enters the steady state (at about t = 10.2 seconds), the three-axis components of both satellite body and the BLDCM rotor no longer have angular velocities.

Further, (3) During the steady state process of attitude control, all three BLDCM rotor speeds approach zero; and, taking the BLDCM in the x-axis attitude component as an example, it can be seen that the three-phase currents (i_a, i_b, i_c) are almost zero due to no more load imposed from the speed.

6.2 Case (II) Attitude Control Analysis

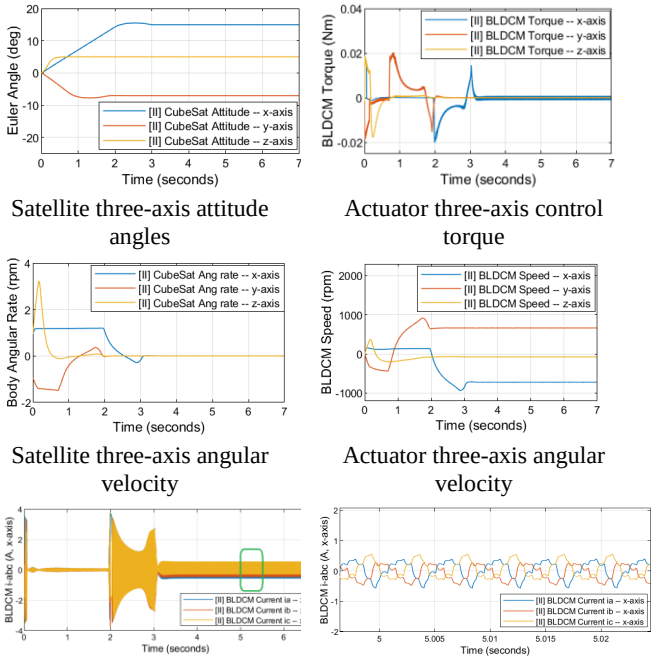

Satellite three-axis attitude angles

Actuator three-axis control torque

Satellite three-axis angular velocity

Actuator three-axis angular velocity

BLDCM three-phase current (i_a, i_b, i_c): (left) full-range, (right) steady state

Figure 22: CubeSat attitude control simulation output results based on Case [II] scenario

Case [II] is to simulate the situation when the satellite body is starting from an attitude angle of [0º, 0º, 0º] with an initial velocity set of [-0.1, 0.1, -0.1] (rad/s), which is then driven to the reference attitude of [15º, -7º, 5º]. From the waveforms of the relevant results shown in Fig.(22), it can be seen that: (1) It is still able to achieve the attitude control target with very small errors (0.07% in x-axis, 0.03% in y-axis, and 0.04% in z-axis) according to the attitude output.

In addition, (2) The three-axis dynamic angular velocity output waveforms between the satellite body and the reaction wheel motors are not completely consistent: Firstly, during the transient process of startup, the angular momentum exchange between the two subsystems results in the same dynamic trend of rotational speed waveforms. Then, as the x-axis completes the attitude tracking and the system enters a steady state (at about t = 3.1 seconds), the satellite body no longer has an angular velocity; in stead, the three x-, y- and z-axes of reaction wheels operate in constant velocities of 663, -76, and 723 (rpm), respectively! Obviously, this is due the result that the reaction wheel receives the initial angular velocity of the satellite body in order to comply by angular momentum conservation of the system.

Further, (3) As mentioned above, after completing the three-axis attitude target and entering the steady state, the rotors of the three BLDCMs still run at constant speeds. And, from the x-axis BLDCM's three-phase currents (ia, ib, ic) shown in Fig.(22), it can be seen that: during ACS's steady state, it still needs to provide current (about 0.5 (A) in amplitude) to the motor to support the load imposed by the rotor rotating at a constant speed.

6.3 Case (III) Attitude Control Analysis

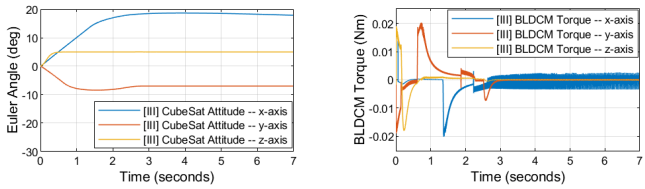

Satellite three-axis attitude angles

Actuator three-axis control torque

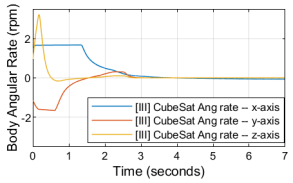

Satellite three-axis angular velocity

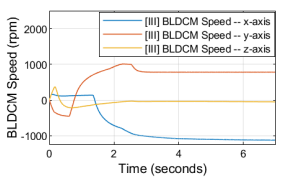

Actuator three-axis angular velocity

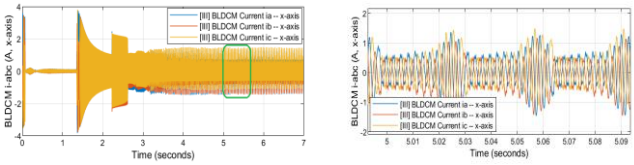

BLDCM three-phase current (i_a, i_b, i_c): (left) full-range, (right) steady state

Figure 23: CubeSat attitude control simulation output

results based on Case [III] scenario

Case [III] is different from case [II] only in that the simulated satellite body is driven with a larger initial velocity set of [-0.15, 0.12, -0.1] (rad/s). From the result waveforms shown in Fig.(23), it can be seen that: (1) The attitude pointing control cannot be achieved effectively in case [III]. Specifically, although the satellite y- and z-axes can complete the reference attitude follow-up, the attitude control goal in x-axis is not reached (or at least in terms of time efficiency); further, the attitude angle of the x-axis in the steady state has a deviation of 2.91º with the error being as high as 19.4%!

In addition, (2) Firstly, similar to that of case [II], during the transient process, the angular momentum exchange between the two subsystems results in same dynamic trend of rotational speed waveforms. Afterwards, along with the y- and z-axes complete the attitude tracking and enter into the steady state (at about t = 3.6 seconds), the angular velocity of the satellite body approaches stationary, and the BLDCM rotors in the three-axis components are still in operation at constant speeds of -1120, 782, -50 (rpm), respectively! Obviously, in addition to the fact that reaction wheels rotate due to angular momentum exchange, the large initial velocity (-0.15 (rad/s)) in the x-axis of the satellite results in big pointing deviation during attitude tracking.

Further, (3) As mentioned above, after completing the three-axis attitude tracking and entering the steady state, the rotors of the three motors still rotate at constant speeds. From the x-axis BLDCM's three-phase currents (ia, ib, ic) shown in Fig.(23), it is clear that: after the ACS reaches a steady state, it still needs to provide current (about 1.5 (A) in amplitude) to the motors to support the load imposed by the rotor rotational movement.

7. Conclusion and Discussion

In this article, the model generated from the CubeSat's electro-mechanical perspectives and concepts of servo control applications can be used as a basis for understanding satellite attitude determination and control system design; in particular, this model is suitable for satellites with active control using BLDCM and reaction wheels. And, Matlab-Simulink is applied to construct a dynamic mathematical model including the CubeSat (kinematics, dynamics) module, the three actuators (BLDCMs and reaction wheels), and the servo motion based controllers for the actuator. More specifically, though the satellite body and the reaction wheel actuator are coupled to each other in cascades, the design of individual controllers are completed based on multi-loop control architecture of "inner current loop/middle angular velocity loop/outer angle loop". Among them, for the satellite body cascade, a "P+PI" type of attitude pointing control law is proposed through closed-loop system response simulation, which can achieve precise attitude pointing in terms of time efficiency, stability and robustness as the system control requirements.

Table 4: Comparison on attitude pointing simulation results

Case	Initial Condition	Attitude Target	BLDCM Power Loss
I	Satellite is stationary	Achieved w/o error	Motor currents (i_a, i_b, i_c) are zero, and power loss ≈ 0. See Fig.(21)
II	Satellite is in rotational motion	Achieved with tiny error	Motor currents (i_a, i_b, i_c) are non-zero, and power loss ≠ 0. See Fig.(22)
III	Satellite initial speed is larger than ($\omega_{critical}$)	Not achieved!	Motor currents (i_a, i_b, i_c) are large, and power loss is high! See Fig.(23)

1) In addition, according to the simulation results of CubeSat attitude control in section (F), the analysis and comparison among cases [I]~[III] are summarized as in Table(4), which reveals following aspects:
2) When proceeding attitude pointing control, if the satellite body is at a standstill (i.e., zero initial angular velocity: $\omega_{x0} = 0$, $\omega_{y0} = 0$, $\omega_{z0} = 0$), not only error-free attitude control can be achieved, but the power loss during the process is also the lowest, regardless during the transient state of startup or the steady state; especially, after the steady state of the attitude goal is reached, both the speed and current of the BLDC motor are zero, and the power loss ≈ 0!
3) In contrast, if the satellite body is still under rotation (that is, it has initial angular velocity: $\omega_{x0} \neq 0$, $\omega_{y0} \neq 0$, $\omega_{z0} \neq 0$), no matter it is the transient state or the steady state, the power loss during the process is obviously increased; Especially, in the steady state after reaching the attitude target, both the speed and current of the actuator motor are not zero, as shown in the result of case [II]. Obviously, this is due the result of angular momentum exchange between the reaction wheel and satellite body; and, the former receives the initial angular velocity of the latter in order to comply with angular momentum conservation of the system.
4) Further, if the initial angular velocity components of the satellite body is greater than the critical value ($\omega_{critical}$) [16, 17], the axis that is beyond the critical initial angular velocity will not be able to track the reference attitude and result in a significant deviation from the pointing target. In the simulation of case [III], the x-axis cannot (or at least not in time efficiency) achieve the goal of attitude control in real time. In addition, the motor speed and current are non-zero, and there is much larger power loss!

Therefore, in the future, based on the active attitude control system using electric motor and reaction wheel, it is necessary to apply a passive actuator (such as a magnetorquer) to complete de-tumbling or 3-axes stabilization operation beforehand, in order to implement the CubeSat precise attitude control and the lowest power loss in the process.

8. Acknowledgements

After decades of career as an engineer, I returned my alma mater to continue my graduate study, and I received a lot of attention and care from teachers, classmates, and colleagues from this department, and I feel warmth as if returning home. Moreover, thanks to the careful guidance and encouragement from Prof. Pan, I can quickly get into track of learning; also, with the assistance and support of Department Chair, Prof. Zhao, I can concentrate on studying. Thank you all very much.

References

[1] National Aeronautics and Space Administration(NASA), "NASA_CubeSat_101_Basic Concept and Process for First-Time CubeSat Developers," NASA CubeSat Launch Initiative, 2017.
[2] Ceren Kaplan, "LEO Satellites-Attitude Determination and Control Components-Some Linear Attitude Control," Thesis, Department of Electrical and Electronics Engineering, Middle East Technical University, April 2006.
[3] Breno Braga Galvao, Maria Cristina Mendes Faustino, Luiz Carlos Gadelha de Souza, "Satellite Attitude Control System Design with Nonlinear Dynamics and Kinemtics," Proceedings of the XXXVII Iberian Latin-American Congress on Computational Methods in Engineering Suzana Moreira Ávila (Editor), ABMEC, Brasília, DF, Brazil, November 6-9, 2016.
[4] Valdemir Carrara1, Hélio K. KugaA, "Torque and Speed Control Loops of A Reaction Wheel," 11th International Conference on Vibration Problems, Lisbon, Portugal, 9-12 September 2013.
[5] Jacoba Aur, "Design of an Aerodynamic Attitude Control System for a CubeSat," Thesis, Department of Electrical and Electronic Engineering, University of Stellenbosch, South Africa, March 2012.
[6] Shiqiao Zhu, "Analysis of Spacecraft Attitude Control," Thesis, Department of Mechanical Engineering and Mechanics, Lehigh University, May 2016.
[7] Blanke, Mogens and Larsen, Martin Birkelund, "Satellite Dynamics and Control in a Quaternion Formulation," Document, Department of Electrical Engineering, Technical University of Denmark, 2010.
[8] Edgard Martínez Vidal, "Development of models for Attitude Determination and Control System components for CubeSat," Thesis, Department of Computer Science, Electrical and Space Engineering, Luleå University of Technology, 2017.
[9] Soner KARATAS, "Attitude Determination and Control Hardware Development for Small Satellites," Thesis, Department of Electrical and Electronics Engineering Middle East Technical University, April 2006.
[10] Kuei-Tsun Chen, "Identification and Restoration of IPMSM Nonlinear EM Characteristics for Motion Control Dynamic Simulation," International Journal of Science and Research (IJSR), December 2019.

[11] Kuei-Tsun Chen, "IPMSM Speed Servo Control Dynamic Simulation," Flotrend Electronics News, December 2018.
[12] 詹前茂, "電機驅動控制理論與實驗", 新文京開發出版股份有限公司, 2003.
[13] Molina Juan Carlos, Ayerdi Víctor, Zea Luis, "Attitude Control Model for CubeSats," Universidad del Valle de Guatemala, Guatemala, 2018.
[14] James Diebel, "Representing Attitude-Euler Angles, Unit Quaternions, and Rotation Vector," Stanford University, California, October 2006.
[15] Paula Sorolla Bayod, "Torque and Speed Control Loops of A Reaction Wheel," Thesis, Universitat Polit`ecnica de Catalunya – BarcelonaTECH, September 2019.
[16] Daniel M. Torczynski and Rouzbeh Amini, "Magnetorquer Based Attitude Control for A Nanosatellite Testplatform," American Institute of Aeronautics and Astronautics (AIAA), 2010.
[17] Lisa Jonsson, "Simulations of Satellite Attitude Maneuvers-Detumbling and Pointing," Thesis, Department of Computer Science, Electrical and Space Engineering, Luleå University of Technology, 2019.

Annex

Annex-(1) Specification data and system parameters of BLDCM for this study

Table 5: BLDCM specification and system parameters

Parameter	Symbol / Name		Value
Geometry Spec.	Slot No.		6
	Stator Outer Diameter		34.4(mm)
	Rotor Outer Diameter		20.0 (mm)
	Air-gap Width		0.5 (mm)
	Stack-length		9.5 (mm)
Winding Spec.	R_s	Phase Resistance	1.1 (Ohm)
	Stator Coil		64 (turn/Ph/Pole)
	Connection Type		Y-Connection
Electrical Spec.	p	Pole No.	4
	f_n	Rated Frequency	333.3 (Hz)
	f_c	Carrier Frequency	10000 (Hz)
	V_{dc}	Input Voltage	6 (VDC)
Parameter	Symbol / Name		Value
Electrical Parameters	L_d	d-axis inductance	0.00104 (H)
	L_q	q-axis inductance	0.00104 (H)
	λ_{pm}	PM Flux	0.0014405 (Wb)
	K_e	BEMF Coefficient	0.000572 (Nm/A)
Mechanical Parameters	J_m	Equivalent MI.	$2.956e^{-7}$ (Kgm^2)
	B_m	Friction Coefficient	$2.66e^{-6}$ (Nm/deg/s)
Controller Parameters	Current Controller	K_{P_d}	34.63
		K_{I_d}	45331
		K_{P_q}	69115
		K_{I_q}	65.35

Annex-(2) Specification data and system parameters of 3U-CubeSat for this study

Table 6: 3U-CubeSat specification and system parameters

Parameter	Symbol / Name	Value
Satellite Moment of Inertia (MI., Kgm^2)	I_{xx}	0.040682055
	I_{yy}	0.040869745
	I_{zz}	0.009426754
	$I_{xy} = I_{yx}$	0.00002119885
	$I_{xy} = I_{zx}$	0.00015089971
	$I_{yz} = I_{zy}$	0.00042680893
Angular-Rate Controller	K_{d_x}	37239
	K_{d_y}	37411
	K_{d_z}	8629
Attitude Controller	K_{p_x}	31.5
	K_{p_y}	31.5
	K_{p_z}	31.5
	K_{i_x}	225
	K_{i_y}	225
	K_{i_z}	225

Abstracts of the Autor's(*Keui-Tsun Chen's*) own reference articles listed in [H. References] of the above submitted manuscript:

[10] Identification and Restoration of IPMSM Nonlinear EM Characteristics for Motion Control Dynamic Simulation

This paper is about identifying electromagnetic (EM) nonlinearities of IPMSM using FEM process; specifically, the extracted nonlinear EM elements are restored into dynamic model for variable speed control simulation. And, for the requirement of being closer to actual IPMSM dynamical behavior, non-ideal aspects such as iron-core saturation and cross-saturation between d-/q- magnetic circuits as well as slot-effects should all be included. The former reveals the temporal harmonics, while the later shows the spatial harmonics. Then, the iron loss resistance (R_i) is introduced by correcting the d-/q- equivalent circuit, so as to account for the magnetic losses associated with the above EM nonlinear elements. In this study, data of these nonlinear elements, such as d-/q- inductances (L_d, L_q), BEMF coefficients (K_e) and cogging torque were extracted through FEM software, which are transformed into "Look-Up Table (LUT)" blocks and setup in the dynamic circuit-control model. This nonlinearized model (as Model-III) can be verified by coupling simulation between FEM(2D) and relevant dynamic model(as Model-IV) with "current output/voltage input" method. Besides, through the implementation of this "identification and restoration" process, the simulation time can be greatly reduced from about 24 hours required by Model-IV to only less than 5 minutes for Model-III, and it still keeps close simulation results between the two models.

[11] IPMSM Speed Servo Control Dynamic Simulation

This article continues the FT027 study on the simulation analysis of the steady-state characteristics of IPMSM. First, it points out that the closed-loop servo system with vector control (such as Fig. (4)) can effectively solve the difficulties of start-up and out of step in permanent magnet synchronous motors. Then, the speed servo control system is explored based on PMSM mathematical model using magnetic field-oriented control scheme and the d-q dynamic equivalent circuit. Further, the control laws are developed through closed-loop system response simulation, and parameters of IPMSM controllers are established according to the multi-loop architecture of "inner current loop/outer speed loop".